Linking permeability to crack density evolution in thermally stressed rocks under cyclic loading

I. Faoro,[1] S. Vinciguerra,[2,3,4] C. Marone,[5] D. Elsworth,[5] and A. Schubnel[6]

Received 12 February 2013; revised 27 March 2013; accepted 29 March 2013.

[1] To improve our understanding of the complex coupling between circulating fluids and the development of crack damage, we performed flow-through tests on samples of Etna basalt and Westerly granite that were cyclically loaded by deviatoric stresses. The basalt was naturally microfractured, while the relatively crack-free Westerly granite was thermally pretreated to 500°C and 800°C to generate microcrack damage. Samples were repeatedly loaded and then unloaded under deviatoric stress paths and ultimately to failure. Permeability and water volume content were measured throughout the loading history together with the differential stress. Permeability decreases at low differential stresses and increases at intermediate differential stresses up to a steady value at failure. We use water volume content as a proxy for fluid storage and show that both permeability and storage evolve with damage and evolution of crack density. We use crack models to represent the evolution of permeability as a function of loading state and are able to independently link it to the observed evolution of deformability, used as an independent measure of crack density. **Citation:** Faoro, I., S. Vinciguerra, C. Marone, D. Elsworth, and A. Schubnel (2013), Linking permeability to crack density evolution in thermally stressed rocks under cyclic loading, *Geophys. Res. Lett.*, *40*, doi:10.1002/grl.50436.

1. Introduction

[2] Understanding and predicting the mechanical behavior of volcanic systems and geothermal reservoirs require a detailed knowledge of the physical properties of rocks and their evolution as a function of stress state, fluid flow, temperature, and deformation history. In particular, the interplay between preexisting crack fabric due to thermal cooling [*Vinciguerra et al*., 2005], cyclic magmatic pressurization, and stressing is a key factor influencing the evolution of mechanical damage and resulting paths to failure. The preexisting crack fabric controls both mechanical and transport properties. These in turn control the interactive feedback of stress and fluid pressures in defining the long-term evolution of volcanic edifices and fault zones where weakening occurs by incremental crack damage under cyclic loading. These effects can promote failure at stresses far below the short-term strength due to differential thermal strains, stress corrosion cracking [e.g., *Heap et al*., 2009; *Heap et al*., 2011], chemical alteration, and other mechanisms.

[3] The development of crack damage influences changes in physical properties, such as permeability, and may be indexed relative to measureable changes in modulus or anomalously low seismic wave velocities [*Vinciguerra et al*., 2005; *Benson et al*., 2006]. Crack densities inverted from velocity and permeability measurements indicate a rapid and progressive closure of cracks with increasing stress together with increasing anisotropy in wave speeds [*Benson et al*., 2007; *Stanchits et al*., 2006]. This significant crack damage controls crack nucleation, propagation, and coalescence and the evolution of permeability during deformation. The increase in crack damage is known to strongly influence the mechanical and fluid flow properties of other crystalline rocks (e.g., Westerly granite) [*Thompson et al*., 2006, and references therein] including analogs to the evolution of fault zones [*Zoback and Byerlee*, 1975; *Mitchell and Faulkner*, 2008; 2012].

[4] Crack damage is strongly controlled by thermal stress histories that influence elastic wave properties [*Nasseri et al*., 2007], permeability [*Simmons and Brace*, 1965; *Kern*, 1982], unconfined compressive strength [*Nagaraja Rao and Murthy*, 2001], Young's modulus [*Daoying et al*., 2006; *Homand-Etienne and Houpert*, 1989; *Takarli and Prince-Agbodjan*, 2008], tensile strength [*Homand-Etienne and Houpert*, 1989], fracture toughness [*Nasseri et al*., 2007; 2010], and porosity [*Glover et al*., 1995; *Takarli and Prince-Agbodjan*, 2008]. This significant influence on physical properties is partly explained not only by the $\alpha-\beta$ quartz phase transition (~570°C) but also by differential deformation between grains of contrasting moduli that occur at all temperatures. Thus, thermal stressing is a convenient experimental pretreatment that generates isotropic and controlled intragranular and intergranular crack damage [*Nasseri et al*., 2009] and is used in our work.

[5] This work explores the influence of incremental crack damage induced by cyclic loading on the mechanical and transport properties of thermally stressed crystalline rocks in shallow crustal conditions that are representative of volcanic edifices and high thermal gradient in the upper crust. The behavior of lava flow basalt from Mt. Etna volcano containing a high level of preexisting crack damage induced by natural thermal cooling [*Vinciguerra et al*., 2005] is contrasted with the response of a crystalline rock, i.e., Westerly granite [*Heap et al*., 2009], with no initial

Additional supporting information may be found in the online version of this article.

[1]Department of Earth Sciences, University of Durham, Durham, UK.
[2]Dipartimento di Scienze della Terra, Università di Torino, Turin, Italy.
[3]Department of Earth Sciences, University of Leicester, Leicester, UK.
[4]British Geological Survey, Environmental Science Centre, Nottingham, UK.
[5]Department of Geosciences and the Energy Institute, Penn State University, University Park, Pennsylvania, USA.
[6]Laboratoire de Geologie-ENS/CNRS, Paris, France.

Corresponding author: S. Vinciguerra, Department of Earth Sciences, University of Leicester, University Road, Leicester LE1 7RH, UK. (sv127@le.ac.uk)

0094-8276/13/10.1002/grl.50436

crack damage. Selected samples of Westerly granite were thermally treated at 500°C and 800°C in order to study the role of induced thermal stressing on increasing crack damage. We use mechanistic models of crack evolution to make constrained predictions of the evolution in porosity and permeability via equivalent medium theories. These observations are used to address important questions regarding the coupled role of damage state and stressing in controlling the transport properties of rocks.

[6] In particular, we address questions such as the following: Is there a critical stress or threshold of crack damage that controls the connectivity of the preexisting crack fabric? What determines the rate of permeability change in microcracked rocks and how is this influenced by microcrack formation and reactivation? Finally, how do microcracks contribute to porosity and permeability evolution as stress increases to failure?

2. Experimental Method

[7] Fluid flow-through tests were conducted on cylindrical samples in a pressure vessel capable of controlling mean and deviatoric stresses. Samples were cyclically loaded by constant increments of the principal stress, σ_1 (deviatoric condition). We explored the evolution of permeability and storage as a function of mechanical damage to the sample.

[8] The principal axial stress σ_1 is applied to the sample via a servocontrolled hydraulic ram with a resolution of 0.01 MPa. Confining stress ($\sigma_2 = \sigma_3$) is applied to the exterior of a latex-sheathed cylindrical sample by the pressure of a confining fluid controlled by a high-precision servocontrolled pressure intensifier. Two additional high precision servocontrolled pressure intensifiers control the end-to-end circulation of fluid (deionized water) through the sample, applying a pressure gradient along the axial length of the specimen [*Samuelson et al.*, 2011; *Faoro et al.*, 2012].

[9] Cylindrical samples measuring 44 mm in diameter and 100 mm in length were prepared and sheathed in a latex jacket to isolate the specimen from the confining fluid. Westerly granite samples were predamaged by heating to 500°C and 800°C at a heating rate of 100°C/h and then cooled to room temperature at a rate of 20°C/h. Experiments were performed at room temperature.

[10] The maximum principal stress σ_1 was incrementally increased by load steps of 10 up to 90 MPa at an axial displacement rate of 5 μm/s, while the confining stress was held constant at 5 MPa (see Supplementary Figure) throughout the whole test. Technical limitations prevented the application of higher confining stresses. In order to allow the samples to relax, they were unloaded after a few cycles of loading by 40 MPa and then reloaded. Fluid was driven through the sample by establishing a differential pore pressure of 3 MPa across the length of the sample. During each load step, the stress was maintained constant for the duration necessary to obtain steady state fluid flow (~3 min). In each experiment, the flow rate was measured via the displacement of the piston within the pressure intensifier.

[11] The permeability of the sample is evaluated from Darcy's law as follows:

$$k = \frac{Q \cdot v \cdot L_s}{A_s \cdot \Delta \mathrm{P}} \tag{1}$$

where k is the permeability (m^2); Q, flow rate (m^3/s); μ, dynamic viscosity (Pa s); L_S, length of the sample (m); A_S, cross-sectional area of the sample (m^2); ΔP, the pore pressure differential over the length of the sample (Pa).

[12] During the loading and unloading stress cycles, when the fluid pressure response is transient, the volumetric water content is evaluated as follows:

$$\Delta V_w = A_{\mathrm{Pi}}(D_{i1} - D_{i2}) - A_{\mathrm{Po}}(D_{o1} - D_{o2}) \tag{2}$$

where A_{Pi} and A_{Po} represent cross-sectional areas of the inlet and outlet pore pressure intensifier pistons, respectively (m^2); D_{i1} and D_{i2} (m), displacements of the inlet pore pressure intensifier piston at the interval time ($t_1 - t_2$); D_{o1} and D_{o2} (m), displacements of the outlet pore pressure intensifier piston at the interval time ($t_1 - t_2$). Confining pressure was held constant and differential stress was cycled to increasingly higher values. The normal load was incremented in a series of increasing steps that were separated by lower values. We measured permeability at the highest and lowest values of differential stress as flow rate reached steady state. These lower values were used to assess deformation and changes in permeability. During the loading and unloading stress ramps, we measured the volume water content.

3. Experimental Results

[13] At low levels of axial loads, changes in flow and poromechanical properties are reversible, as the same values of permeability are observed at the beginning and at the end of each loading cycle (see Supplementary Material). As failure is approached, significant and permanent changes in permeability and poromechanical properties are observed, as mirrored in the mismatch between the dramatic decrease in the inlet flow rate and the modest increase in the outlet flow rate. A high angle (~60°) shear fracture formed for all samples.

[14] Permeability for basalt samples (Figures 1a and 1b) loaded at axial stresses between 40 and 60 MPa shows a common decreasing trend from initial values of 5×10^{-17} m^2 to values of 2×10^{-17} m^2. At higher axial stresses, permeability increases up to values of the order of 9×10^{-17} m^2 at the peak stress (i.e., 92 MPa).

[15] Permeability of the pristine Westerly granite sample (p2457) shows a constant value of about 3×10^{-19} m^2 up to axial stress values of 60 MPa. A steady increase in permeability is then observed when approaching failure, with a maximum value of 2×10^{-18} m^2 found at 110 MPa (Figures 1c and 1d). These values are in good agreement with the values of permeability obtained by *Mitchell and Faulkner* [2008] and *Zoback and Byerlee* [1975] in companion studies of cyclic loading at slightly higher effective pressure (10 and 15 MPa) and about 1 order of magnitude higher than those obtained at higher confinements (40 MPa) The permeability for the 500°C thermally treated sample (p2459) increases from an initial magnitude of 4×10^{-18} to 1×10^{-16} m^2 at the peak stress of 100 MPa, about 10% higher than the peak stress observed for Etna basalt samples (Figures 1c and 1d). Permeability for the 800°C thermally treated sample (p2453) decreases

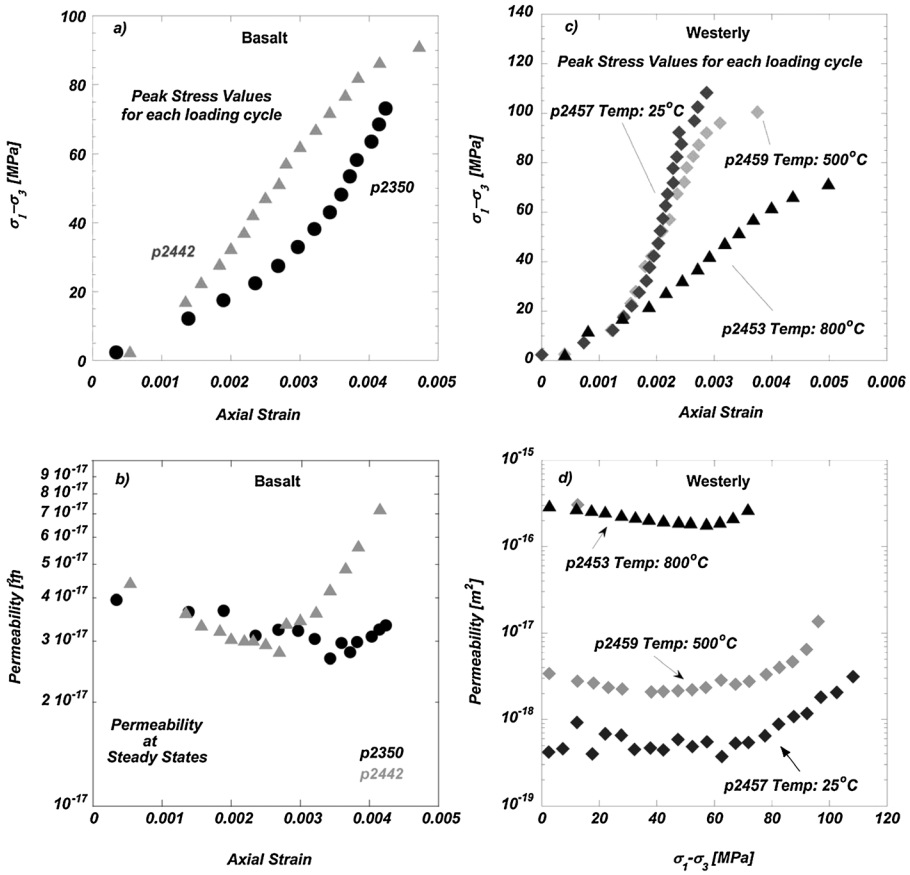

Figure 1. (a) Evolution of the average peak values of axial stress as a function of axial strain for each loading cycle on Etna basalt. (b) Evolution of permeability as a function of axial strain for each loading cycle on Etna basalt. (c) Evolution of the average peak values of stress as a function of axial strain for each loading cycle on Westerly granite. (d) Evolution of permeability as a function of axial deviatoric stress for each loading cycle on Westerly granite.

linearly by about 22% from the initial value of 3×10^{-16} to 2×10^{-16} m^2 at 72 MPa (Figures 1c and 1d). This implies that the thermally treated samples are significantly more cracked and weaker than the pristine samples. The reduction of strength is about 10% for the sample thermally treated at 500° C and about 30% for the sample thermally treated at 800°C, and it is due to the formation of cracks under thermal stress. Cracks become particularly abundant for heat treatment above 570°C, i.e., the temperature equilibrium of the α–β transition of quartz.

[16] For all the samples, the variation of the water volume content (i.e., porosity) mimics that of the permeability trend, i.e., first decreasing during elastic loading (due to crack closure) and then significantly increasing beyond the onset of dilatancy, as brittle failure is approached.

4. Analysis

[17] We explore the use of models to link the evolution of permeability in the cracked solid with the mechanical characteristics of the crack network embedded within the sample. In particular, we link mechanistic models of crack evolution and resulting changes in porosity and permeability with independent measurements of deformation modulus and permeability. We consider and compare the results from the basalt sample p2442 (the only sample loaded to failure) with those from the Westerly thermally treated samples.

4.1. Obtaining crack density from elastic moduli

[18] For an isotropic matrix containing a random distribution of cracks, the effective Young's modulus (or shear modulus) of a rock E^* is a linear function of the crack density, which can be written in the following form:

$$\frac{E_0}{E^*} = 1 + hp \tag{3}$$

[19] In equation (3), ρ is the crack density, defined by $p = \frac{1}{V}\sum_0^N {c_i}^3$, where c_i is the radius of the ith crack, N is the total number of cracks embedded in the representative elementary volume V, E_0 is the Young's modulus of the crack-free matrix, and h is a positive scaling parameter that depends on the matrix and fluid properties, the geometry of the cracks, and the interactions between them. This scalar h has been calculated by many authors for a wide variety of crack geometries and fluid properties. Here we use $h = \frac{16\left(1-\upsilon_0{}^2\right)}{3\pi(1-\upsilon_0/2)}$, which is appropriate for noninteractive penny-shaped cracks [*Kachanov*, 1994; *Schubnel and Guéguen*, 2003]. Using an initial Poisson ratio of ~0.25 yields an h of ~1.9.

[20] One of the more straightforward and least controversial methods is *Kachanov's* [1994] noninteractive effective medium theory, because it neglects stress interactions

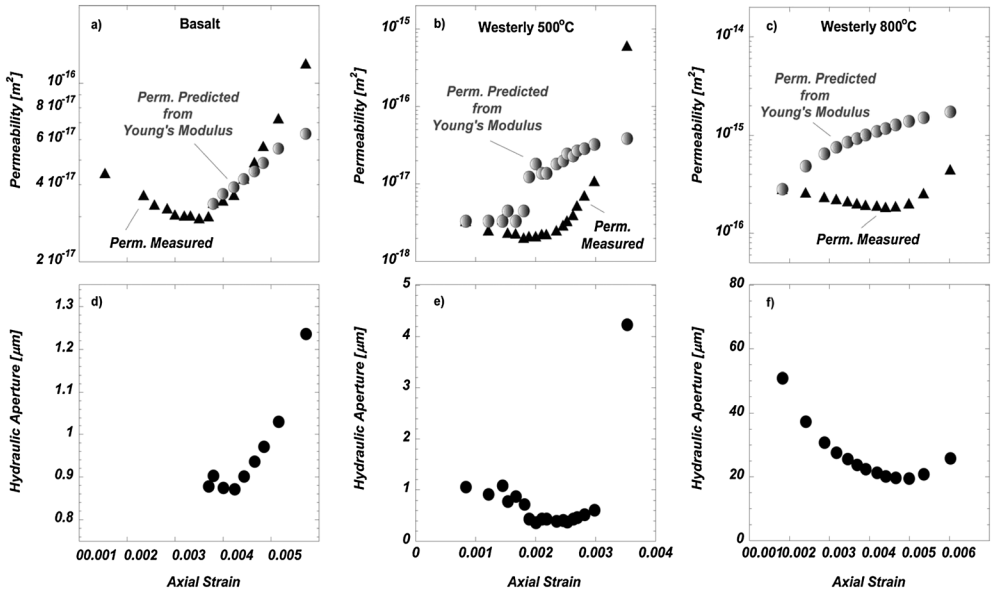

Figure 2. (a–c) Comparison of permeability predicted from Young's modulus and measured during the experiment for Etna basalt (Figure 2a), Westerly granite thermo-treated at 500°C (Figure 2b), and Westerly granite thermally treated at 800°C (Figure 2c). (d–f) Predicted hydraulic apertures as a function of axial strain for Etna basalt (Figure 2d), Westerly granite thermo-treated at 500°C (Figure 2e), and Westerly granite thermo-treated at 800°C (Figure 2f).

between cracks and is considered a valid approximation for low crack densities (up to ~0.5) in the case of either random or aligned crack distributions [*Kachanov*, 1994; *Schubnel*, 2002; *Guéguen and Schubnel*, 2003]. For a random distribution of crack centers and orientations, *Kachanov* [1994] showed that the effective Young's modulus E^* of a dry rock can be written as follows:

$$\frac{E_0}{E^*} = 1 + \frac{p}{3h}\left(1 + \frac{3}{10}\upsilon_0\right) \tag{4}$$

[21] Here we use the approximation of dry cracks, because our experiments measured the static Young's moduli under drained conditions. We note that if the medium is perfectly poroelastic, then the dry moduli are equal to the drained moduli [*Rice and Cleary*, 1976].

[22] We were able to graphically determine the tangent Young's modulus values from all the hysteresis loading loops of the thermo-treated specimens on Westerly granite, but only nine times from the basalt specimen (from 50 MPa to failure) and zero times from the sample on untreated Westerly. Using equation (4) and for an initial Young's modulus E_0 of 50 GPa for the crack-free matrix, we can then unequivocally recover the evolution of crack density as a function of damage at each step of our experiments. It is important to note that because we measure the tangent moduli, which in fact also include reversible inelastic deformation (such as crack sliding and backsliding) [*David et al.*, 2012], we need to use a quite low initial value for E_0.

4.2. Predicting the permeability from crack density

[23] *Guéguen and Dienes* [1989] showed that the effective microcrack network of a porous rock can be represented by an array of penny-shaped cracks embedded in the host matrix, with the bulk rock permeability k given by

$$k = \frac{2}{15} f \omega^2 \zeta p \tag{5}$$

[24] In equation (5), $\zeta = \omega/c$ and ω are the crack average aspect ratio and hydraulic aperture, respectively, and f is the percolation factor. The relation between f and crack density is complex [*Guéguen et al.*, 1997; *Guéguen and Schubnel*, 2003], but we note that f can take any value between zero (all cracks are isolated and unconnected) and unity (all cracks are connected into the network). For the sake of simplicity, we assume that our samples are in the connected regime (so that $f = 1$) and that both the hydraulic aperture and the aspect ratio are constant during the experiment.

[25] This is to say that all variations of permeability are in fact solely due to variations in crack density (i.e., crack length and number). In such a case, equation (5) simplifies to

$$\frac{k}{k_o} \approx \frac{p}{p_o} \tag{6}$$

so that the permeability evolution is easily predicted (with respect to the major assumptions noted above) as a function of the crack density evolution. This includes the additional crack growth induced by volume change because of the α–β quartz transition.

[26] Figures 2a–2c compare the laboratory measurements and the prediction of equation (6).

[27] The agreement is good for the basalt (Figure 2a), with both curves showing increasing permeability with increasing differential stress (Young's modulus values compute starting from 50 MPa of differential stress). This indicates that much of the increase in permeability during dilatancy, for stresses above about 50 MPa, can be explained by the growth of microcracks at constant aspect ratio rather than by a change in connectivity or hydraulic crack aperture.

[28] For the Westerly specimen thermally treated at 500°C (Figure 2b), however, the theoretical permeability inferred from the Young's modulus evolution is always higher than that measured experimentally. In particular, the model predicts an earlier increase in permeability. This discrepancy possibly highlights a percolation effect, i.e., that in fact the permeability k does not vary linearly with crack density but that initially the crack network is not fully connected so that the permeability increases very slowly until some critical threshold after which it increases very fast [*Nara et al*., 2011].

[29] For the Westerly specimen thermally treated at 800°C (Figure 2c), the model overestimates the crack connectivity and consequently the values of permeability.

[30] The predictions of the model and experimental data can be perfectly reconciled when also taking into account possible variations in hydraulic aperture. Indeed, the difference between the measured permeability and predicted permeability can be interpreted in terms of variation of the average hydraulic crack aperture (assuming the crack aspect ratio is constant and equal to 10^{-3} throughout the test) [*Guéguen and Dienes*, 1989].

[31] Figures 2d–2f show the evolution of hydraulic aperture for all three specimens. For the basalt, it is about 1 μm and does not vary significantly. It is of the same order of magnitude for the Westerly granite sample heat treated to 500°C but does increase when approaching failure. Note that this is a lower bound, as close to failure the crack aspect ratio also decreases due to crack propagation. For the Westerly granite specimen thermally treated to 800°C, an average hydraulic aperture of about 1 order of magnitude larger (50 μm) than that from basalt is needed. This is consistent with grain boundary opening due to the α–β quartz phase transition and microstructural observations made by *Nasseri et al*. [2007]. This implies that the cracks are fully opened, with their wall surface not being in contact. As a consequence, it is important to consider the hydraulic aperture as it varies significantly throughout the test: It first decreases in the early stage of the test due to elastic crack closure and then increases when cracks start to propagate.

5. Discussion and Conclusions

[32] The permeability data reported in this study for the Etna basalt show trends similar to those obtained by *Vinciguerra et al*. [2005] at isostatic stress. However, the absolute magnitudes of permeability are offset by about 1 order of magnitude. This offset is attributed to the heterogeneity of the lava flows and the influence of different compositions and cooling rates encountered during their formation.

[33] The evolution of Etna basalt permeability with stress as it approaches failure illustrates that there are three principal trends: (i) In the range of 3–40 MPa, the permeability decays from 5×10^{-17} to 2×10^{-17} m^2 because of the compaction/closure of the interconnected crack network. (ii) Above 60 MPa, the crack damage increases and results in a permeability increase to 9×10^{-17} m^2. (iii) Between 40 and 60 MPa, the permeability remains constant at a minimum value of 2×10^{-17} m^2 because crack closure counterbalances the increasing damage.

[34] These interpretations are supported by the observed variations of the water volume content ($\Delta V_w/V_s$) and the Young's modulus of the samples. In particular, the volumetric water content mirrors the behavior of the inner void space of the specimen. During the initial phase (until 40 MPa), the stress induces closure of the free paths between the interconnected voids (decreasing of the permeability) that, due to the pressure acting on the matrix, expand, decreasing the content of the water in the sample. After 40 MPa, the progressive reopening and new formation (after 60 MPa) of free paths reactivate the circulation of fluid, increasing the content of water in the matrix. At the same time, the rock becomes progressively weaker and a Young's modulus reduction of 30% is observed.

[35] Permeability of Etna basalt is extremely sensitive to the loading conditions. Deviatoric loading closes preexisting voids, particularly the more compliant preexisting high aspect ratio cracks, and results in a rapid decrease in permeability. Upon unloading, the permeability does not fully recover, indicating that the change in permeability is controlled by anelastic processes that permanently alter the transport properties of the microcrack network. Irrecoverable porosity reduction induced by mechanical stress is apparent in tests where the principal axial stress increases from 3 to 42 MPa. Under deviatoric loading, preferential shear loading on unfavorably aligned cracks causes shear dilation and crack extension. The stress sensitivity found is in good agreement with the time-dependent deformation processes observed for Etna basalt and cyclically observed in the volcano at the field scale [*Heap et al*., 2011] after episodes of magma pressurization and dyke intrusion. It is plausible that increasing stress leads initially to a reduction in crack aperture that restricts the rate of transport of reactive species to crack tips and that further stress is required to open major fractures, as indicated by the delayed opening of eruptive fracture systems in the field [*Heap et al*., 2011].

[36] We then qualitatively compare the hydraulic transport characteristics of Etna basalt with naturally and thermally treated Westerly granite, and in particular our results show that the basalt permeability values fall between those recovered from Westerly samples heated at 800°C and 500°C. In particular, during the prefailure portion of the test, only the Westerly sample heated at 500°C shows the same parabolic permeability trend exhibited by the basalt, but with values that are ~1 order of magnitude lower. The results demonstrate that the microstructure of erupted lava flows exhibits significantly different physical properties in comparison with rocks formed in an intrusive environment. Episodes of fast thermal stressing due to dyke emplacement are likely to induce new microcracking in solidified intrusive bodies that are ubiquitous in active volcanoes edifices, such as Etna basalt with increasing crack damage. Different cooling rates and microstructures are likely to affect the absolute magnitude of the transport properties.

[37] We predicted the permeability evolution by analyzing the behavior of an effective microcrack network embedded in the host matrix [*Gueguen and Dienes*, 1989]. The model explains the increase in permeability in terms of crack growth rather than a change in crack properties for the Etna basalt, while an overestimation of permeability that can be ascribed to the variation of the crack aperture/aspect ratio is found for the Westerly granite. The different cooling rates at which the cracks formed are believed to have a profound influence on their geometry features and connectivity and consequently on the critical level of crack damage required before the deformation starts to accelerate to failure, leading to the formation of eruptive fracture systems.

[38] **Acknowledgments.** This work was partially supported by the U.S. Department of Energy under project DOE-DE-FG36-04GO14289 and the National Science Foundation under projects EAR-0510182 EAR-0746192 and OCE-0648331. T. Mitchell is acknowledged for his constructive criticism, which greatly improved the paper.

References

Benson, P., A. Schubnel, S. Vinciguerra, C. Trovato, P. G. Meredith, and P. R. Young (2006), Physical and transport properties of isotropic and anisotropic cracked rocks under hydrostatic pressure, *J. Geophys. Res.*, *111*, B04202, doi:10.1029/2005JB003710.

Benson, P. M., B. D. Thompson, P. G. Meredith, S. Vinciguerra, and R. P. Young (2007), Imaging slow failure in triaxially deformed Etna basalt using 3D acoustic-emission location and X-ray computed tomography, *Geophys. Res. Lett.*, *34*, L03303, doi:10.1029/2006GL028721.

Daoying, X., T. Yuezhan, L. Ting, and X. Songlin (2006), Experimental investigations of thermal damage for rocks. *Key Eng. Mat.* 324–325 II, 1213–1216, doi:10.4028/www.scientific.net/KEM.324-325.1213.

David, E., N. Brantut, A. Schubnel, and R. W. Zimmermann (2012), Sliding crack model for nonlinearity and hysteresis in the uniaxial stress–strain curve of rock, *Int. J. Rock Mec. Min. Sci.*, *52*, 9–17, doi:10.1016/j.ijrmms.2012.02.001.

Faoro, I., D. Elsworth, and C. Marone (2012), Permeability evolution during dynamic stressing of dual permeability media, *J. Geophys. Res.*, *117*, B01310, doi:10.1029/2011JB008635.

Glover, P. W. J., P. Baud, M. Darot, P. G. Meredith, S. A. Boon, C. M. Leravalec, I. S. Zoussi, and T. Reuschle (1995), Alpha/beta phase transition in quartz monitored using acoustic emissions, *Geophys. J. Int.*, *120*(3), 775–782.

Guéguen, Y., and J. Dienes (1989), Transport-properties of rocks from statistics and percolation, *Math. Geol.*, *21*(1), 1–13.

Guéguen, Y., T. Chelidze, and M. Le Ravalec (1997), Microstructures, percolation thresholds, and rock physical properties, *Tectonophysics*, *279*, 23–35.

Guéguen, Y., and A. Schubnel (2003), Elastic wave velocities and permeability of cracked rocks, *Tectonophysics*, *370*, 163–176.

Kachanov, M. (1994), Elastic solids with many cracks and related problems, *Adv. Appl. Mech.*, *30*, 259–445.

Kern, H. (1982), Elastic-wave velocity in crustal and mantle rocks at high pressure and temperature: the role of the high-low quartz transition and of dehydration reactions, *Phys. Ear. Plan. Int.*, *29*(1), 12–23.

Heap, M. J., S. Vinciguerra, P. G. Meredith (2009), The evolution of elastic moduli with increasing crack damage during cyclic stressing of Etna basalt. *Int. J. Rock Mech. Min. Sci*, *471*, 161–169, doi:10.1016/j.tecto.2008.10.004.

Heap, M. J., P. Baud , P. G. Meredith, S. Vinciguerra, A. F. Bell, I. G. Main (2011), Brittle creep in basalt from Mt Etna volcano: implications for time-dependent volcano deformation, *Earth Planet. Sci. Lett*, *307*(1-2), 71–82, doi:10.1016/j.epsl.2011.04.035.

Homand-Etienne, F., and R. Houpert (1989), Thermally-induced microcracking granites: characterization and analysis, *Int. Rock Mech. Min. Sci. Geomech. Abstr.*, *26*(2), 125–134.

Mitchell, T. M., and D. R. Faulkner (2008), Experimental measurements of permeability evolution during triaxial compression of initially intact crystalline rocks and implications for fluid flow in fault zones, *J. Geophys. Res.-Solid Earth*, *113*, B11412, doi:10.1029/2008JB005588.

Mitchell, T. M., and D. R. Faulkner (2012), Towards quantifying the matrix permeability of fault damage zones in low porosity rocks, *Earth Planet. Sci. Lett*, *339–340*, 24–31, doi:10.1016/j.epsl.2012.05.014.

Nagaraja Rao, G. M., and C. R. L. Murthy (2001), Dual role of microcracks; toughening and degradation, *Can.Geotech. J.*, *38*(2), 427–440.

Nara, Y., P. G. Meredith, T. Yoneda, and K. Kaneko (2011), Influence of macro-fractures and micro-fractures on permeability and elastic wave velocities in basalt at elevated pressure, *Tectonophysics*, *503*(1-2), 52–59, doi:10.1016/j.tecto.2010.09.027.

Nasseri, M. H. B., A. Schubnel, and R. P. Young (2007), Coupled evolutions of fracture toughness and elastic wave velocities at high crack density in thermally treated Westerly Granite, *Int. J. Rock Mech. Min. Sci.*, *44*(4), 601–616, doi:10.1016/j.ijrmms.2006.09.008.

Nasseri, M. H. B., A. Schubnel, P. M. Benson, R. P. Young (2009), Common evolution of mechanical and transport properties in thermally cracked westerly granite at elevated hydrostatic pressure, *Pure Appl. Geophys*, *166*(2009), 927–948, doi:10.1007/s00024-009-0485-2.

Nasseri, M. H. B., G. Grasselli, B. Mohanty (2010), Experimental relationship between fracture toughness and fracture roughness in anisotropic granitic rocks, *J. Rock Mech*, *43*(4), 403–415, doi:10.1007/s00603-009-0071-z.

Rice, J. R., and M. P. Cleary (1976), Some basic stress diffusion solutions for fluid-saturated elastic porous-media with compressible constituents, *Rev. Geophys*, *14*(2), 227–241.

Samuelson, J., D. Elsworth, and C. Marone (2011), Influence of dilatancy on the frictional constitutive behavior of a saturated fault zone under a variety of drainage conditions, *J. Geophys. Res.*, *116*, B10406, doi:10.1029/2011JB008556.

Schubnel, A., (2002), Mécanique de la dilatance et de la compaction des roches de la croûte, *Thèse de doctorat*, Institut de Physique du Globe de Paris, 229 pp.

Schubnel, A., and Y. Guéguen (2003), Dispersion and anisotropy of elastic waves in cracked rocks. *J. Geophys. Res.*, *108*(B2), doi:10.1029/2002JB001824.

Simmons, G., and W. F. Brace (1965), Comparison of static and dynamic measurements of compressibility of rocks, *J. Geophys. Res.*, *70*(22), 5649–5656.

Stanchits, S., S. Vinciguerra, G. Dresen (2006), Ultrasonic velocities, Acoustic emission characteristics and crack damage of basalt and granite, *Pure Appl. Geophys*, *163*, 1–20, doi:10.1007/s00024-006-0059-5.

Takarli, M., and W. Prince-Agbodjan (2008), Temperature effects on physical properties and mechanical behavior of granite: Experimental investigation of material damage, *J. ASTM Int.*, *5*(3), 13, doi:10.1520/JAI100464.

Thompson, B. D., R. P. Young, and D. Lockner (2006), Fracture in westerly granite under AE feedback and constant strain rate loading: Nucleation, quasi-static propagation, and the transition to unstable fracture propagation, *Pure Appl. Geophys.*, *163*, 995–1019, doi:10.1007/s00024-006-0054-x.

Vinciguerra, S., C. Trovato, P. G. Meredith, and P. M. Benson (2005), Relating seismic velocities, permeability and crack damage in interpreting the mechanics of active volcanoes, *Int. J. Rock Mech*, *42*(7-8), 900–910, doi:10.1016/j.ijrmms.2005.05.022.

Zoback, M. D., and J. D. Byerlee (1975), Effect of microcrack dilatancy on permeability of westerly granite, *J. Geophys. Res.*, *80*, 752–755.